

# REENTRY HEATING ANALYSIS OF SPACE SHUTTLE

## WITH COMPARISON OF FLIGHT DATA

Leslie Gong, Robert D. Quinn, and William L. Ko  
Dryden Flight Research Facility  
NASA Ames Research Center  
Edwards, California

### SUMMARY

Surface heating rates and surface temperatures for a space shuttle reentry profile were calculated for two wing cross sections and one fuselage cross section. Heating rates and temperatures at 12 locations on the wing and 6 locations on the fuselage are presented. The heating on the lower wing was most severe, with peak temperatures reaching values of 1240°C for turbulent flow and 900°C for laminar flow. For the fuselage, the most severe heating occurred on the lower glove surface where peak temperatures of 910°C and 700°C were calculated for turbulent flow and laminar flow, respectively.

Aluminum structural temperatures were calculated using a finite difference thermal analyzer computer program, and the predicted temperatures are compared to measured flight data. Skin temperatures measured on the lower surface of the wing and bay 1 of the upper surface of the wing agreed best with temperatures calculated assuming laminar flow. The measured temperatures at bays 2 and 4 on the upper surface of the wing were in quite good agreement with the temperatures calculated assuming separated flow. The measured temperatures on the lower forward spar cap of bay 4 were in good agreement with values predicted assuming laminar flow. However, temperatures measured on the aft spar cap were higher than the values calculated for laminar flow. The upper spar cap temperatures computed for separated flow were in fairly good agreement with the flight data.

### INTRODUCTION

The space shuttle orbiter is designed to be used for approximately one hundred flights. During each flight the vehicle must withstand severe aerodynamic heating during reentry through the atmosphere. The space shuttle skin and substructure are constructed primarily of aluminum which must be protected during reentry with a thermal protection system (TPS) from being overheated beyond the design temperature limit of 177°C so that the integrity of the structure is maintained for subsequent flights.

In addition to the temperature limit, the temperature gradient within the structure must not be too severe or the resulting thermal stress will buckle the skin and cause possible bondline failure.

In order to gain confidence in the thermal protection system, re-entry heating analysis of the shuttle must be made and the temperature distribution within the structure must be estimated to assure that the design temperature is not exceeded and the thermal stresses are not excessive.

This paper presents calculated surface (aerodynamic) heating rates and surface temperatures for the wing at wing station (WS) 240 and wing station (WS) 328. Also presented are the aerodynamic heating rates and surface temperatures computed for six locations on the fuselage at fuselage station (FS) 877. Wing stations 240 and 328, and FS 877 were chosen for analyses because these locations were most heavily instrumented. In addition, calculated aluminum skin and spar cap temperatures for the wing at WS 240 are shown and compared to available measured flight data.

#### SYMBOLS

H	altitude, m
Q	heating rate, $\frac{kw}{m^2 \cdot sec}$
T	temperature, °C
V	velocity, $\frac{m}{sec}$
$\alpha$	angle of attack, degrees

#### SPACE SHUTTLE

A planform view and side view of the space shuttle showing the two wing locations and one fuselage location for which aerodynamic heating analyses were made are shown in figure 1. As shown, calculations were made for WS 240, WS 328, and FS 877. A thermal model was also made for the wing cross section at WS 240 and structural temperatures were calculated for this location. Cross sections of the wing at WS 240 and WS 328, and the fuselage at FS 877 showing the general moldline geometry are presented in figure 2.

## FLIGHT CONDITIONS

In order to make aerodynamic heating calculations, time histories of altitude, Mach number or velocity, and angle of attack must be determined. For the present investigation the nominal STS-1 (Space Transportation System) reentry flight trajectory shown in figure 3 was used. Also shown in this figure are the actual reentry flight time histories of angle of attack, velocity, and altitude. As can be seen the two trajectories are in excellent agreement and, therefore, calculations made using the nominal trajectory can be used to compare with flight data.

## DESCRIPTION OF WING STRUCTURE

The geometry of the wing section at WS 240 for which structural temperatures were calculated is shown in figure 4. Both the upper and lower skins and forward spar web of bay 1 are made of aluminum honeycomb sandwich plates. The skins for bays 2, 3, and 4 are made of spanwise "hat" stringer reinforced aluminum skins. The remaining spar webs are made of corrugated aluminum. The lower wing skin is covered with high temperature reusable surface insulation (HRSI), with the strain isolation pad (SIP) lying between the wing skin and the HRSI. Most of the upper skin of bay 1 is protected by low temperature reusable surface insulation (LRSI) under which lies the SIP layer. The HRSI and LRSI are bonded to the SIP with room temperature vulcanized (RTV) silicone rubber and the SIP is bonded to the skin with RTV. The remainder of the upper skin of bay 1 and all of the upper skin of bays 2, 3, and 4 are covered with felt reusable surface insulation (FRSI). The FRSI is bonded directly to the skin, with RTV, and there is no SIP layer.

## CALCULATING METHODS

### Aerodynamic Heating

External heating rates and surface temperatures were computed by the DFRC computer program "THEOSKN". This program solves the one-dimensional thin skin heating equation and computes time-histories of heating rates, temperatures, heat transfer coefficients, skin friction, etc. At present this program can compute turbulent heat transfer by the theory of van Driest (reference 1) and Eckert's reference enthalpy method (reference 2), and laminar heat transfer by Eckert's reference enthalpy method (reference 2). Also, 3-D stagnation point laminar heat transfer and 2-D stagnation point laminar heat transfer with and without sweep can be computed by the theory of Fay and Riddell (reference 3). The swept cylinder theory of Beckwith and Gallagher (reference 4) is used to compute turbulent stagnation point heating.

The local flow conditions used in the heating equations can be computed by the program or can be input to the program from some other source. At present, the program can calculate normal shock local flow with or without sweep, and local flow conditions based on the oblique shock theory, the Prandtl-Meyer expansion theory, and/or the tangent cone theory. Also, heating rates can be arbitrarily changed by user input, and a transition number based on Reynolds number and/or Mach number may be input to the program to change heating calculations (e.g. laminar to turbulent flow). All calculations are based on real gas properties of air.

In the present investigation, heating rates and surface temperatures were calculated for the upper and lower surfaces of the wing at WS 240 and WS 328, and for the fuselage at FS 877. Three cases of heating rates and surface temperatures were calculated for the wing at WS 240. Namely, (i) turbulent flow for both the lower and upper surfaces, (ii) laminar flow for both the lower and upper surfaces, and (iii) laminar flow for the lower surface and bay 1 of the upper surface, and separated flow for the aft bays of the upper surface. For WS 328, heating rates and surface temperatures were computed only for case iii. The laminar heating rates were computed by Eckert's reference enthalpy method, and the turbulent heating rates were computed by the theory of van Driest. For both cases a Reynolds analogy factor of 1.12 was used. The local flow conditions were computed by the oblique shock theory and the Prandtl-Meyer expansion theory. The initial wedge angle was taken to be 30 degrees. The flow distance was the chordwise distance measured from the leading edge of the wing. The laminar and turbulent heating rates for the upper surface were computed by the same procedure used to calculate the lower surface heating rates except that the flow expansion was limited in such a way that the local static pressures did not go below three-tenths of the free stream static pressure. Finally, the separated flow heating rates for the upper surface were estimated. For this analysis, the separated flow heating rates were taken to be one-half of the attached laminar flow calculated heating rates.

Heating rates and surface temperatures were calculated for the lower surface of the fuselage by the turbulent swept cylinder theory of Beckwith and Gallagher and the laminar swept cylinder theory of Fay and Riddell. Calculations for the lower glove surface were also made using the above theories. However, the resulting heating rates were increased by 20 percent as suggested by results from wind tunnel tests (references 5 and 6). For the leading edge of the "glove," only laminar calculations were made using the swept cylinder theory of Fay and Riddell. The upper "glove" surface was known to be in a low heating separated flow region. Measured results for similar geometry on the X-15 airplane during a reentry flight (reference 7) showed the lower surface heating to be about thirty times the upper surface heating. Therefore, the heating rates for the upper glove surface were estimated by taking one-thirtieth of the heating rates calculated for the lower "glove" surface. For the side of the fuselage, it was assumed that the flow was separated from the fuselage glove junction to a point (attachment point) on the fuselage where the TPS changed from

FRSI to LRSI. This location is about halfway up the side of the fuselage. Heating rates and surface temperatures were calculated for the side of the fuselage using Eckert's reference enthalpy method for laminar flow and assuming that the local attached flow conditions were equal to free stream values. The separated flow heating rates on the side of the fuselage were assumed to be equal to one-tenth the attached flow calculations. The heating rates and surface temperatures for the upper fuselage surface were computed by Eckert's reference enthalpy method for laminar flow with and without transition at a local Reynolds number of  $5 \times 10^5$ . The local flow conditions were calculated using the Prandtl-Meyer expansion theory with initial flow conditions equal to free-stream values. The flow distance was measured from the attachment point on the side of the fuselage. Two calculations were made. In the first calculation, the local flow was allowed to expand until the local static pressure was equal to one-half the free stream pressure. In the second calculation, the local static pressure was limited to one-fourth the free stream value.

### Structural Temperature Calculations

The structural temperatures were computed using the Lockheed Thermal Analysis program (reference 8). This program computes transient temperature distributions in configurations of arbitrary complexity, using the electrical resistance capacity analogy. Solutions are obtained by converting the physical system into one consisting of lumped thermal capacitors connected by the thermal resistors and then using the lumped-parameter, or finite-difference approach, to solve for the temperature history of the system. This program permits direct solutions of complex transient problems involving conduction, convection, radiation, and heat storage. Furthermore, since it is also possible to specify any quantity as an arbitrary function of any other, it is also possible to solve such problems as change of state, variable thermodynamic properties, arbitrary variable boundary conditions (such as aerodynamic heating) and other non-linear effects. Input format is not restricted to any particular geometry, but is such that resistors and capacitors can be connected in any manner desired.

When using this program to compute temperatures for a large thermal model, it is desirable to make the computing interval as large as possible so that the computational time is not excessive. The computing interval for this program is determined by multiplying the minimum RC product by a given factor. The default value of this multiplying factor is 0.25. The RC product is the product of the capacity of a lump times the equivalent resistance of that lump, and the equivalent resistance is the parallel combination of all the resistors connected to the lump. The multiplying factor of 0.25 can be changed to any desired value. However, care must be exercised, as too large a computing interval will result in unreliable results. In the present investigation, a multiplying factor of 0.9 was used which resulted in a computing interval of approximately 1.0 second.

The thermal properties of the TPS and aluminum structure are functions of pressure and/or temperature and therefore must be updated at frequent intervals if good results are to be obtained. In the present analysis, the thermal properties were updated at each computing interval (1.0 second). Also when calculating the conduction resistors, the temperature used to update the conductivity was the average of the temperature of the two lumps connected by the resistor.

## THERMAL MODEL

The third bay of the wing cross section at WS 240 was first modeled by a one-dimensional thermal model. One of the primary purposes for making the one-dimensional calculations was to determine how many layers<sup>1</sup> (lumps) the HRSI should be divided into in order to get a good solution with minimum computer running time. Consequently, the thermal model was made with the HRSI divided into 5, 10 and 15 layers. The thermal model with the HRSI divided into 10 layers is shown in figure 5. The circled numbers are the lump numbers, and numbers on the right are the resistors connecting the lumps. Resistors 1 through 14 and 16 through 19 are the conduction resistors. Resistor 15 is the internal radiation resistor and 26 and 27 are the external radiation resistors which radiate to the free-stream temperature  $T_{\infty}$ . The results from the one-dimensional calculations are presented in figure 6 which shows a plot of the maximum calculated lower skin temperatures versus the number of HRSI layers. As shown, the temperature difference between the 5 layer model and 15 layer model is 1.67°C. However, the difference between the 10 and 15 layer model is only 0.27°C and is insignificant. Based on these calculations, it was decided that for all subsequent thermal models, the HRSI would be divided into approximately 10 layers.

The two dimensional thermal model for the entire wing cross section, excluding the leading edge and elevon, at WS 240 is shown in figures 7, 8, and 9. As shown in figure 7, the TPS and aluminum structure were divided into 410 lumps (capacitors). Figure 8 shows the conduction resistors and the external radiation resistors. There are a total of 486 conduction resistors and 45 external radiation resistors. Also shown in figure 8 are the aerodynamic heating inputs which are denoted by the arrows labeled Q20 to Q41, and Q50 to Q71. Because of the gaps in the reusable surface insulation (RSI), heat conduction was allowed only in the RSI thickness direction. As shown in figure 8, each external lump radiated to the ambient temperature  $T_{\infty}$ . The emissivity used to compute the radiation heat flux was 0.85 for the lower surface and 0.80 for the upper surface. Also the view factor used in the radiation calculations

<sup>1</sup>In this discussion, the word layers refers to lumps in the TPS thickness direction. Therefore, for the one-dimensional thermal model, the two words are synonymous.

was 1.0. Typical internal radiation resistors are shown in figure 9. There are a total of 553 internal radiation resistors. View factors were computed for each internal radiating lump, and the emissivity used in the heat flux calculations was 0.667.

## RESULTS AND DISCUSSION

### Heating Rates and Surface Temperatures

Wing - The surface heating rates calculated for wing station 240 are shown in figure 10. Turbulent and laminar heating rates were computed for the lower surface and bay 1 of the upper surface. For bays 2, 3, and 4 of the upper surface, turbulent, laminar, and separated heating rates were calculated. Details of the methods used to compute the heating rates and surface temperatures are presented in the previous section of this paper called CALCULATING METHODS. The turbulent heating rates are shown by the solid lines. The laminar heating rates are shown by the dashed lines, and the heating rates computed for separated flow are shown by the long and short dashed lines. For the lower surface, the maximum heating rate calculated, assuming turbulent flow, varied from  $225 \text{ kw/m}^2\text{-sec}$  at bay 1 to  $175 \text{ kw/m}^2\text{-sec}$  at bay 4. For laminar flow, the maximum heating rate varied from  $75 \text{ kw/m}^2\text{-sec}$  at bay 1 to  $40 \text{ kw/m}^2\text{-sec}$  at bay 4. The maximum upper surface heating rate computed for turbulent flow was  $5.9 \text{ kw/m}^2\text{-sec}$ , and for laminar flow was  $5.8 \text{ kw/m}^2\text{-sec}$ . The heating rates calculated assuming separated flow varied from a maximum of  $2.2 \text{ kw/m}^2\text{-sec}$  at bay 2 to  $1.6 \text{ kw/m}^2\text{-sec}$  at bay 4. It may be noted that the laminar heating rates computed for the upper surface are higher than the turbulent heating rates for the first 1000 seconds of the reentry trajectory, and the total heating rates calculated for turbulent flow are only slightly higher than the total laminar heating rates. This apparent abnormality is due to the very low Reynolds numbers on the upper surface of the wing.

The calculated surface temperatures for the lower surface at WS 240 are shown in figure 11. The maximum temperatures calculated for turbulent flow vary from  $1240^\circ\text{C}$  at bay 1 to  $1090^\circ\text{C}$  at bay 4. For laminar flow, the maximum temperatures vary from  $900^\circ\text{C}$  at bay 1 to  $690^\circ\text{C}$  at bay 4. The upper surface temperatures are shown in figure 12. The maximum surface temperature occurs at bay 1 and is  $315^\circ\text{C}$ . It may also be noted that the maximum calculated temperatures for turbulent flow and laminar flow are nearly the same. The surface temperatures computed for separated flow range from  $165^\circ\text{C}$  at bay 2 to  $120^\circ\text{C}$  at bay 4.

Calculated heating rates for WS 328 are shown in figure 13. The laminar flow heating rates computed for the lower surface of the wing reached maximum values of  $85 \text{ kw/m}^2\text{-sec}$  at bay 1 and  $53 \text{ kw/m}^2\text{-sec}$  at bay 3. For the upper surface, the heating rates were computed assuming laminar flow for bay 1 and separated flow for bays 2 and 3. The maximum heating rate at bay 1 is  $6 \text{ kw/m}^2\text{-sec}$ , and for bays 2 and 3 the maximum heating rates are slightly above  $2 \text{ kw/m}^2\text{-sec}$ .

The surface temperatures at WS 328 are shown in figure 14 for the lower surface and figure 15 for the upper surface. All of the lower surface temperatures and the temperatures for bay 1 of the upper surface were calculated assuming laminar flow. The temperatures for bay 2 and bay 3 of the upper surface were computed assuming separated flow. The lower surface reaches maximum temperatures of  $880^\circ\text{C}$ ,  $800^\circ\text{C}$ , and  $740^\circ\text{C}$  at bays 1, 2, and 3 respectively. For the upper surface, the maximum temperature at bay 1 is  $370^\circ\text{C}$ , and the peak temperatures at bays 2 and 3 are  $230^\circ\text{C}$  and  $208^\circ\text{C}$ , respectively.

Fuselage - Heating rates at six locations on the fuselage at FS 877 are presented in figure 16. Calculations are shown for location 1 (lower fuselage centerline), location 2 (lower surface of the glove), location 3 (leading edge of the glove), location 4 (upper surface of the glove), location 5 (side of the fuselage), and location 6 (top centerline of the fuselage). Details of the methods used to make these calculations are discussed in the previous section called CALCULATING METHODS. At location 1, heating rates are shown for both laminar and turbulent flow. The maximum value obtained for turbulent flow was  $100 \text{ kw/m}^2\text{-sec}$  and the peak laminar heating rate calculated was  $48 \text{ kw/m}^2\text{-sec}$ . Turbulent and laminar heating rates are also shown for location 2. The peak heating rate for turbulent flow is  $115 \text{ kw/m}^2\text{-sec}$  and for laminar flow is  $45 \text{ kw/m}^2\text{-sec}$ . It should be mentioned that the turbulent calculated heating rates at location 2 were empirically increased by 20 percent as discussed in the previous section. However, this empirical factor was not applied to the laminar calculations. At location 3, only laminar flow heating rates were calculated and as shown, the peak value at this location is  $80 \text{ kw/m}^2\text{-sec}$ . Two curves of calculated heating rates assuming separated flow are shown for location 4. The lower curve represents the estimated heating rates that were expected at this location. However, because of the uncertainty of the heating at this location, due to the complex flow field on the upper glove, conservative estimates of the heating rates were also made and are shown by the upper curve. At location 5, heating rates were generated assuming separated flow and assuming attached laminar flow with transition to turbulent flow at 1350 seconds. The attached flow calculations produced

a peak heating rate of  $14 \text{ kw/m}^2\text{-sec}$ . However, if the flow is assumed separated at location 5, the maximum heating rate is  $1.4 \text{ kw/m}^2\text{-sec}$ . Two curves of calculated heating rates are shown for location 6. The lower curve was computed assuming laminar flow and also assuming that the local static pressures were equal to one-fourth of the free-stream values. As shown, this curve reaches a peak value of  $4 \text{ kw/m}^2\text{-sec}$ . The upper curve was computed assuming laminar flow with transition to turbulent flow at a Reynolds number of  $5 \times 10^5$  (time = 1050 seconds) and also assuming that the local static pressures were equal to one-half the free-stream values. The maximum heating rate shown by this curve is  $8 \text{ kw/m}^2\text{-sec}$ .

Surface temperatures calculated for the same six locations at which the heating rates were computed are shown in figure 17. As shown, the heating at locations 1, 2, and 3 is quite severe with peak temperature at location 1 and location 2 reaching approximately  $910^\circ\text{C}$  for turbulent flow and  $700^\circ\text{C}$  for laminar flow. At location 3 the peak temperature is  $850^\circ\text{C}$ . The temperatures at location 4 reached peak values of  $190^\circ\text{C}$  and  $275^\circ\text{C}$  depending on which heating rate curve was used (see figure 16). The maximum surface temperature calculated at location 5 was  $157^\circ\text{C}$  if separated flow was assumed and  $450^\circ\text{C}$  if the flow is assumed to be attached. The surface temperatures at location 6 reached a peak value of  $325^\circ\text{C}$  when it was assumed that the flow transitioned to turbulent flow at 1050 seconds.

### Structural Temperatures

Predicted aluminum skin temperature time histories at four locations on the lower surface of the wing at WS 240 are shown in figure 18 and figure 19. Also shown for comparison are STS-1 measured flight temperatures. Figure 18 shows the skin temperatures for bays 1 and 2, and figure 19 shows the skin temperatures for bays 3 and 4. Except for bay 3 (figure 19), flight data for the time interval 0 to 1178 seconds were not available due to telemetering "blackout." Calculated temperatures are shown for turbulent flow using 80 percent TPS thickness, laminar flow using 80 percent TPS thickness, and laminar flow using 100 percent TPS thickness. Eighty (80) percent of the TPS thickness was used to account for gap heating effects<sup>2</sup>. As shown, the measured data falls about halfway between the two laminar curves up to 1650 seconds of the flight profile, and it is apparent that the flow on the lower surface of the wing was laminar. The fact that data falls midway between the two laminar curves indicates that the effect of gap heating may not be as severe as that imposed on the calculations by using 80 percent TPS thickness. It is obvious from

<sup>2</sup>The 80 percent TPS thickness was the design criterion used by space shuttle manufacturer to account for the effects of gap heating.

the comparisons shown in figure 18 and 19 that good agreement between the measured and calculated data up to 1650 seconds of the flight profile would have been obtained if 90 percent TPS thickness had been used in the calculations. After 1650 seconds, the flight data shows an increasing deviation from the calculated values and the agreement between the measured and calculated data is poor. The result was expected since the forced convection cooling from 1550 seconds to touchdown at 1916 seconds was not accounted for in the calculations (see figure 10). Also after touchdown the free convection external cooling and the free convection internal heating were neglected in the calculations.

Comparisons between measured and calculated skin temperatures on the upper surface of the wing are shown in figures 20 and 21. Skin temperature time-histories for bays 1 and 2 are shown in figure 20, and skin temperature time-histories for bay 3 and bay 4 are shown in figure 21. Calculated temperatures are shown for turbulent flow using 80 percent TPS thickness and laminar flow using 80 percent TPS thickness. Also shown are temperatures computed assuming laminar flow and 100 percent TPS thickness for bay 1 and temperatures calculated for separated flow with 100 percent TPS thickness for bays 2, 3 and 4. For bay 1, it can be seen that the measured flight data are in quite good agreement with the temperatures calculated assuming laminar flow and 100 percent TPS thickness. At bays 2 and 4, the temperatures calculated assuming separated flow and 100 percent TPS thickness are in fairly good agreement with the measured flight data. It may be noted that the measured temperatures at bays 2 and 4 continue to increase after touchdown. This increase in temperature of the upper skins is due to convection and radiation heating from the hotter lower skins. The upper skin of bay 1 does not show this increase in temperature after touchdown because the skins of bay 1 are made of aluminum honeycomb core sandwich plates which insulates the thermocouple, located on the outer skin, from the internal heating effects.

Comparisons between measured and calculated temperatures on the lower spar caps are shown in figure 22. The flight data for the lower forward spar cap of bay 4 are in good agreement with the laminar flow curve for 80 percent TPS thickness up to 1800 seconds. It may be noted that the measured skin temperatures at bay 4 (see figure 19) do not agree as well with the calculated values as do the measured temperatures of the forward spar cap. This somewhat poorer agreement between the measured and calculated skin temperatures may result from the fact that the skin was actually made of "hat" stringer reinforced aluminum, whereas, the skin used in the thermal model was an equivalent flat plate. The measured temperatures for the rear spar cap are higher than the laminar flow curve for 80 percent TPS thickness. The lower predicted values for the aft spar cap are probably due to the assumption of total insulation of the aft side of the rear spar web. Like the lower skin data, the flight data for the lower spar caps level off and remain virtually constant after 1800 seconds.

Comparisons between measured and calculated temperatures on the upper spar caps are shown in figure 23. As was the case for the upper skin temperatures, the measured flight data for the spar caps agree best with the values calculated assuming separated flow and 100 percent TPS thickness. The measured data show a higher rate of increase after touchdown than predicted by the calculated curve, and this higher heating rate is probably due to the effects of internal convection which were neglected in the calculations.

#### CONCLUDING REMARKS

A transient aerodynamic heating program was used to compute time-histories of surface heating rates and surface temperatures for two wing cross sections and one fuselage cross section. The heating on the lower surface of the wing was most severe, with peak temperatures reaching values of 1240°C for turbulent flow and 900°C for laminar flow. For the fuselage, heating was most severe at the lower glove surface where the peak temperatures were 910°C for turbulent flow and 700°C for laminar flow.

A finite-difference thermal analyzer computer program was used to compute structural temperatures for a wing cross section at WS 240. The predicted structural temperature time-histories were compared with measured flight data. These comparisons showed that, for the first 1650 seconds of the reentry trajectory, the temperatures measured on the lower surface of the wing were in fair agreement with values calculated assuming laminar flow. After 1650 seconds the flight data deviates from the predicted values due primarily to the fact that the external convection cooling and the internal convection heating were neglected in the calculations. The temperatures measured on the upper surface at bay 1 were in quite good agreement with values computed assuming laminar flow, and the upper surface temperatures measured aft of bay 1 were in fairly good agreement with values calculated assuming separated flow. The differences that do exist between the measured and calculated temperatures on the upper surface of the wing and the lower surface of the wing prior to time 1650 seconds could be caused by the following assumptions made in the thermal model: (1) the use of effective thickness for the TPS to account for gap heating; (2) initial temperatures and emissivities; (3) total insulation of the aft and forward spar webs; (4) the use of effective thickness for stiffened skin, corrugated spar webs, and honeycomb core skins; (5) no internal convection; and (6) the two-dimensional nature of the thermal model.

## REFERENCES

1. van Driest, E. R.: The Problem of Aerodynamic Heating, *Aeronautical Engineering Review*, Vol. 15, No. 10, pp. 26-41, Oct. 1956.
2. Eckert, E. R. G.: Survey of Boundary Layer Heat Transfer at High Velocities and High Temperatures, WADC Technical Report 59-624, Wright Air Development Center, U.S. Air Force, April 1960.
3. Fay, J. A.; and Riddell, F. R.: Theory of Stagnation Point Heat Transfer in Disassociated Air, *Journal of Aeronautical Science*, Vol. 25, No. 2, pp. 73-85, 121, Feb. 1958.
4. Beckwith, I. E.; and Gallagher, J. J.: Local Heat Transfer and Recovery Temperatures on a Yawed Cylinder at a Mach Number of 4.15 and High Reynolds Numbers, NASA TR R-104, 1961 (Superceeds NACA Memo 2-27-59L).
5. Space Shuttle Aerothermodynamics Technology Conference, Volume I - Flow Fields, NASA TM X-2506, Feb. 1972.
6. Space Shuttle Aerothermodynamics Technology Conference, Volume II - Heating, NASA TM X-2507, Feb. 1972.
7. Quinn, R. D.; and Olinger, F. V.: Heat Transfer-Measurements Obtained on the X-15 Airplane with Correlation with Wind Tunnel Results, NASA TM X-1905, 1969.
8. Thermal Analyzer Computer Program for the Solution of General Heat Transfer Problems, LR 18902, Lockheed California Company, July 1965.

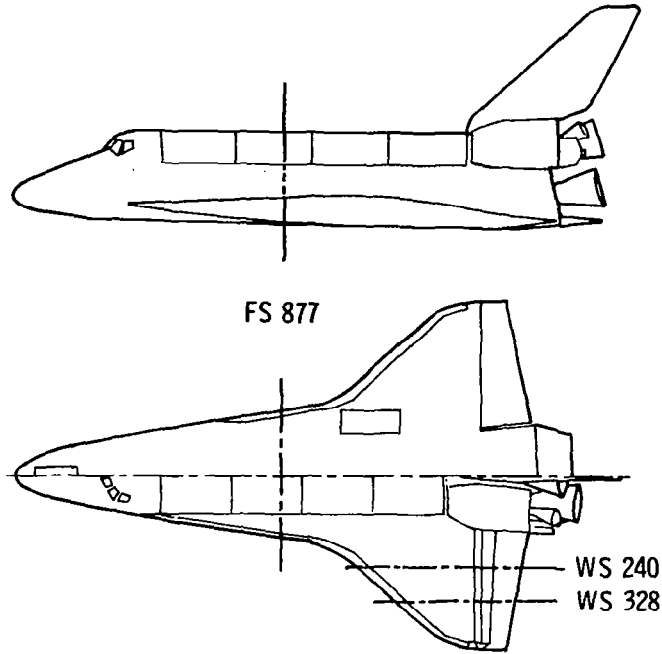


Figure 1.- Wing and fuselage locations analyzed.

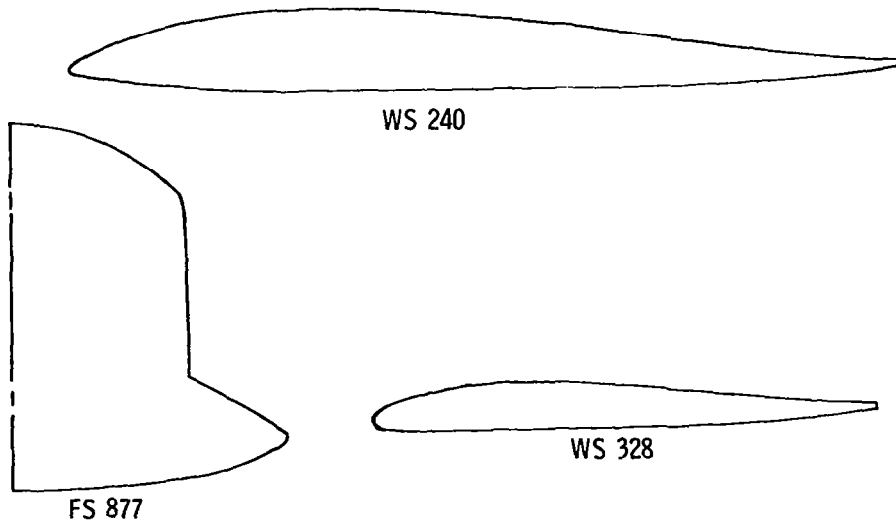


Figure 2.- Wing and fuselage cross sections.

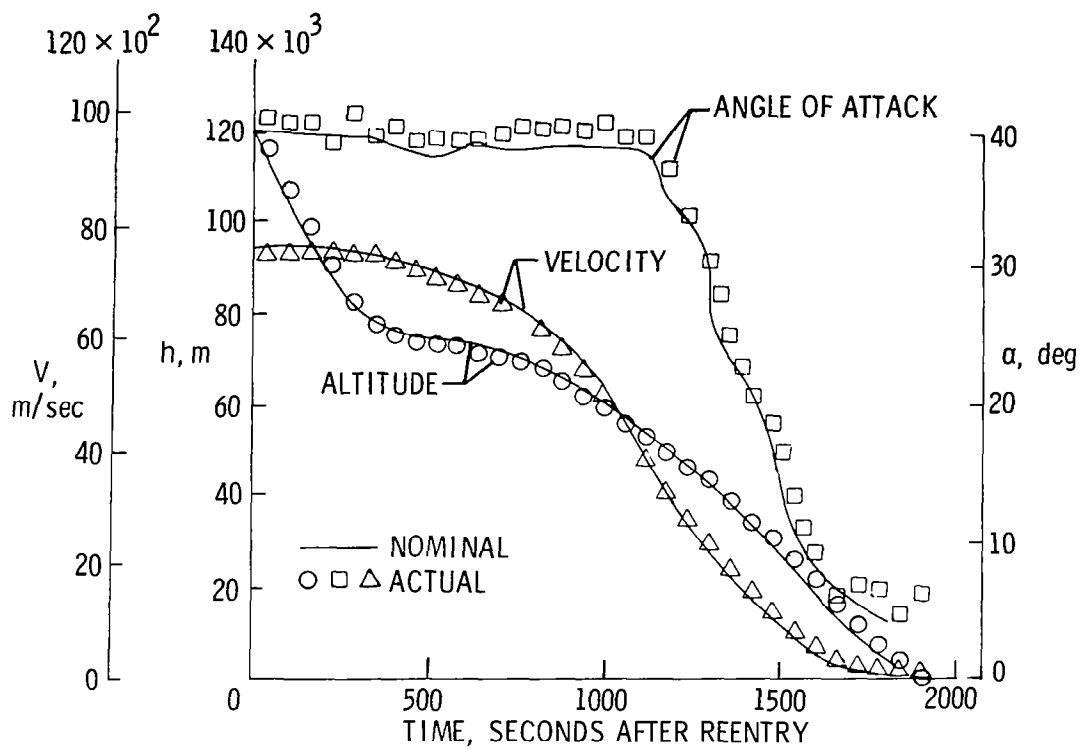


Figure 3.- Flight time histories.

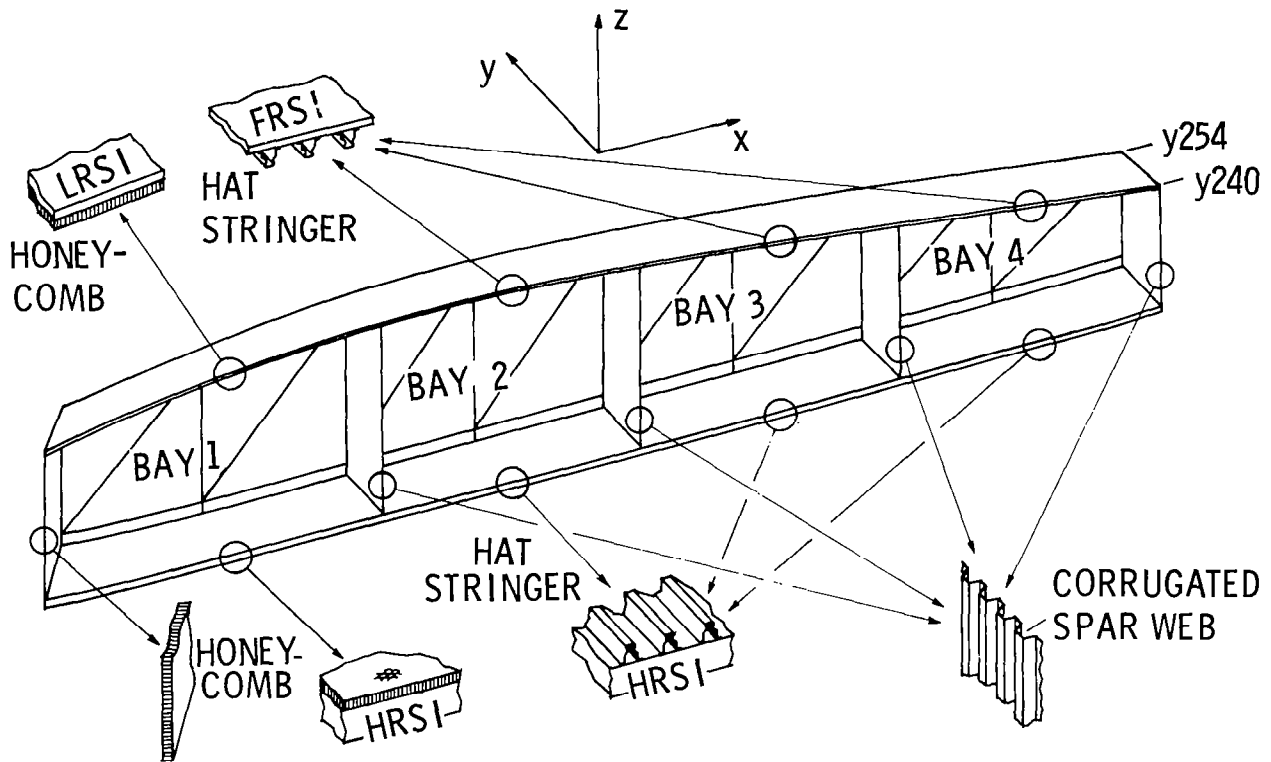


Figure 4.- Geometry of wing at WS 240.

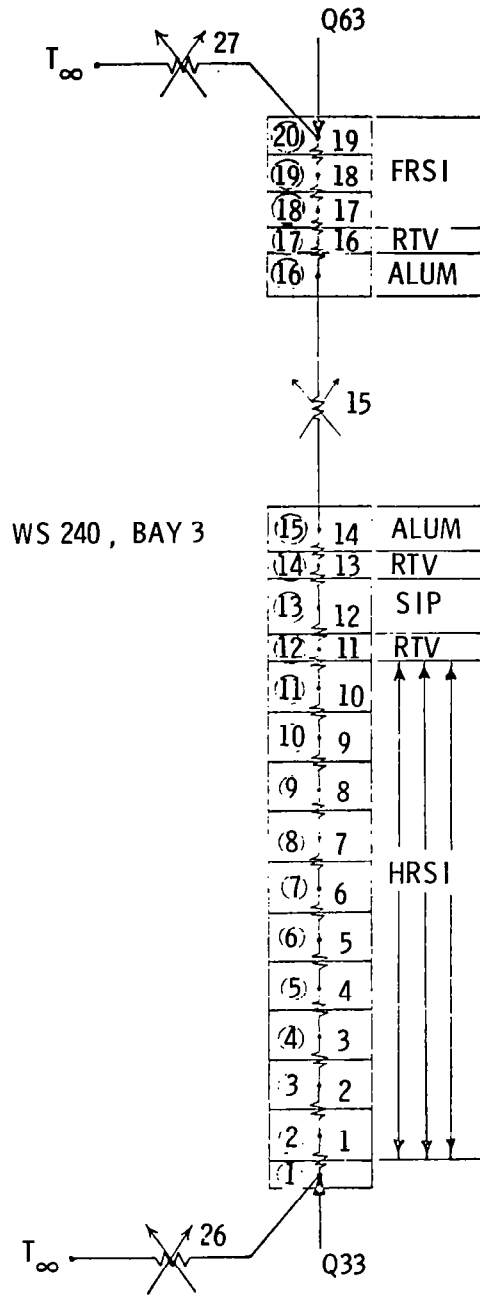


Figure 5.- One-dimensional thermal model.



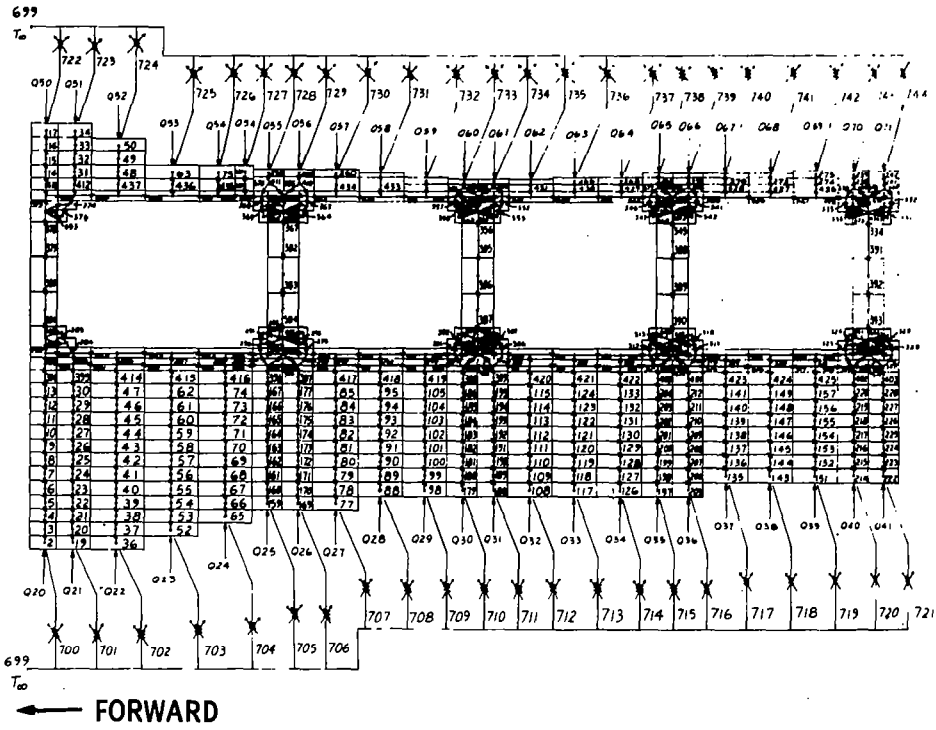


Figure 8.- Thermal model, resistors at WS 240.

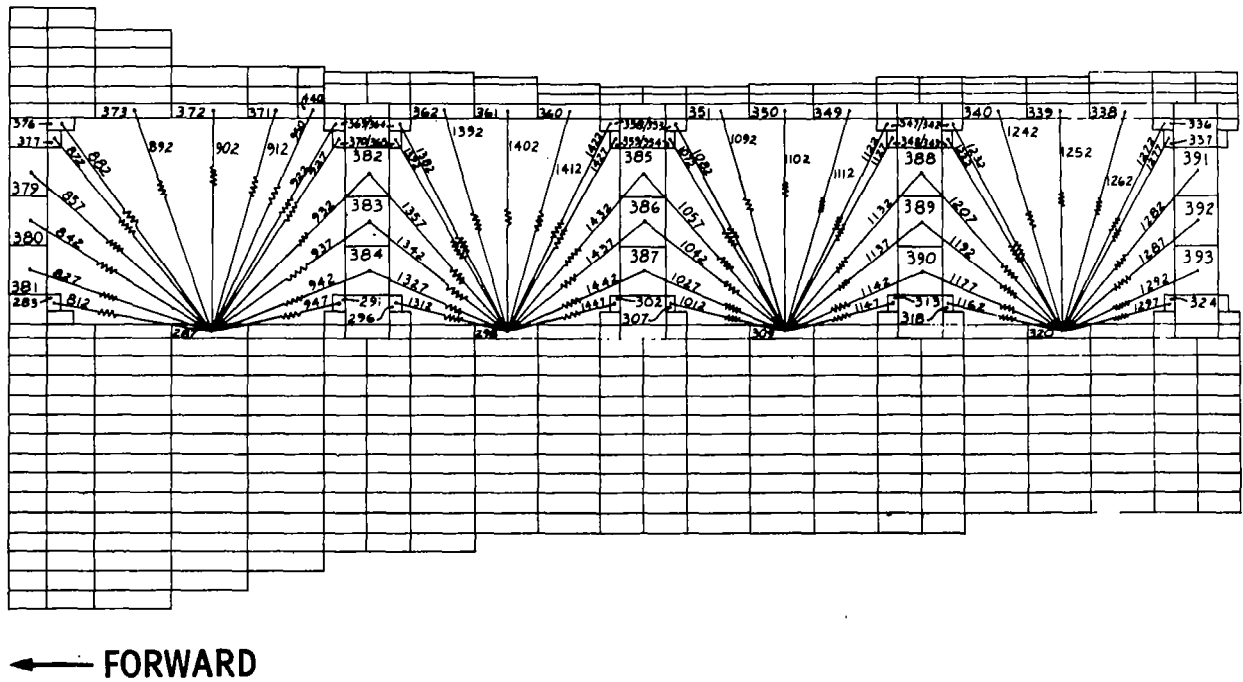


Figure 9.- Thermal model, internal radiation at WS 240.

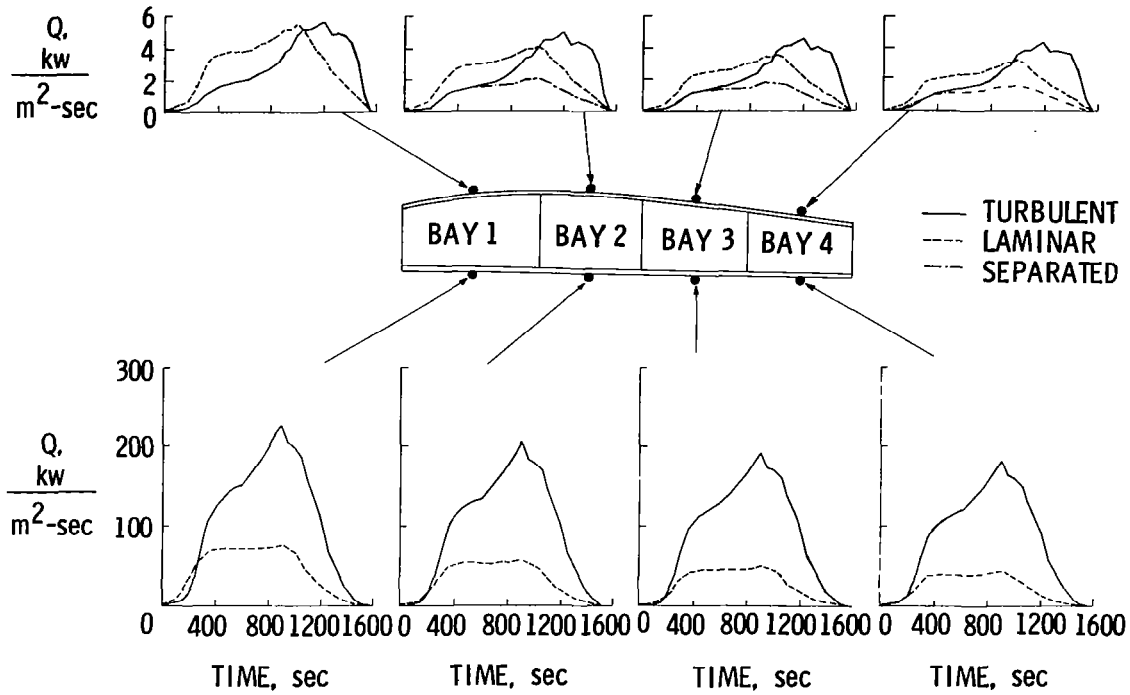


Figure 10.- Calculated heating rates, WS 240.

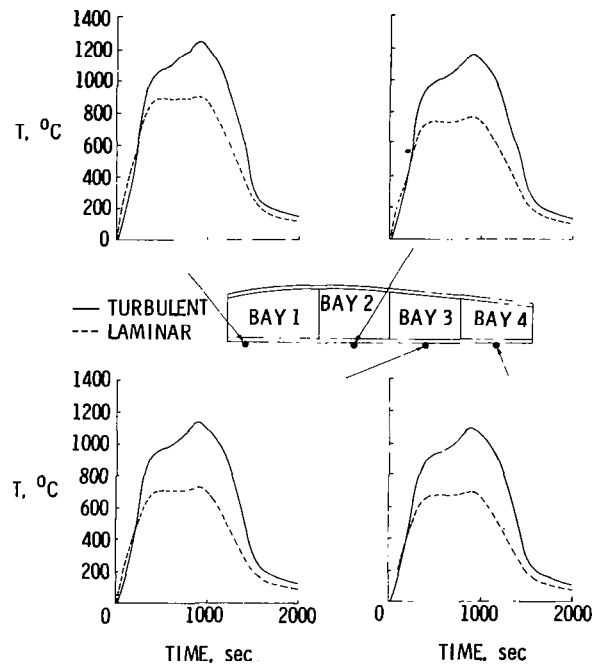


Figure 11.- Calculated surface temperatures of lower surface, WS 240.

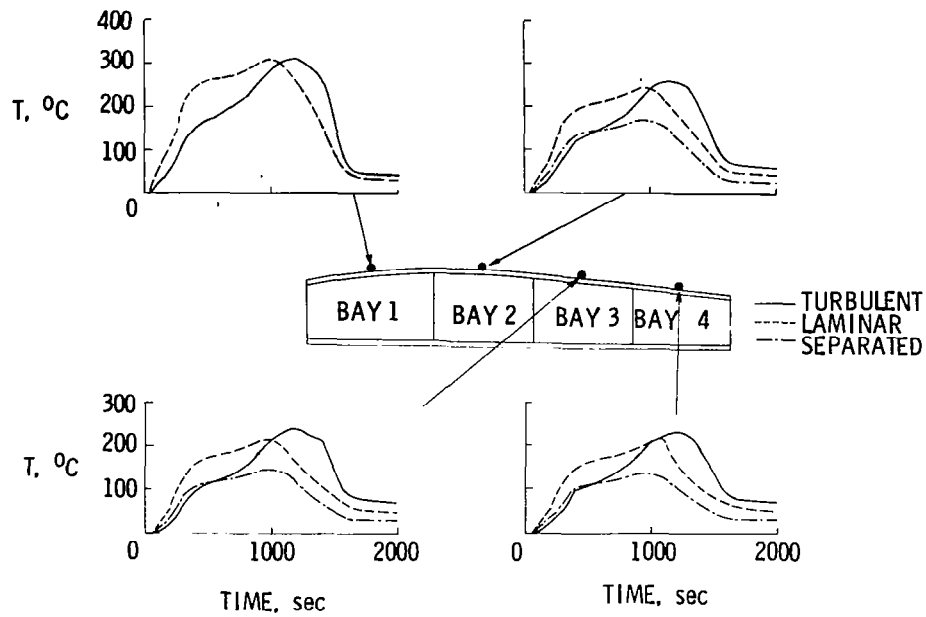


Figure 12.- Calculated surface temperatures of upper surface, WS 240.

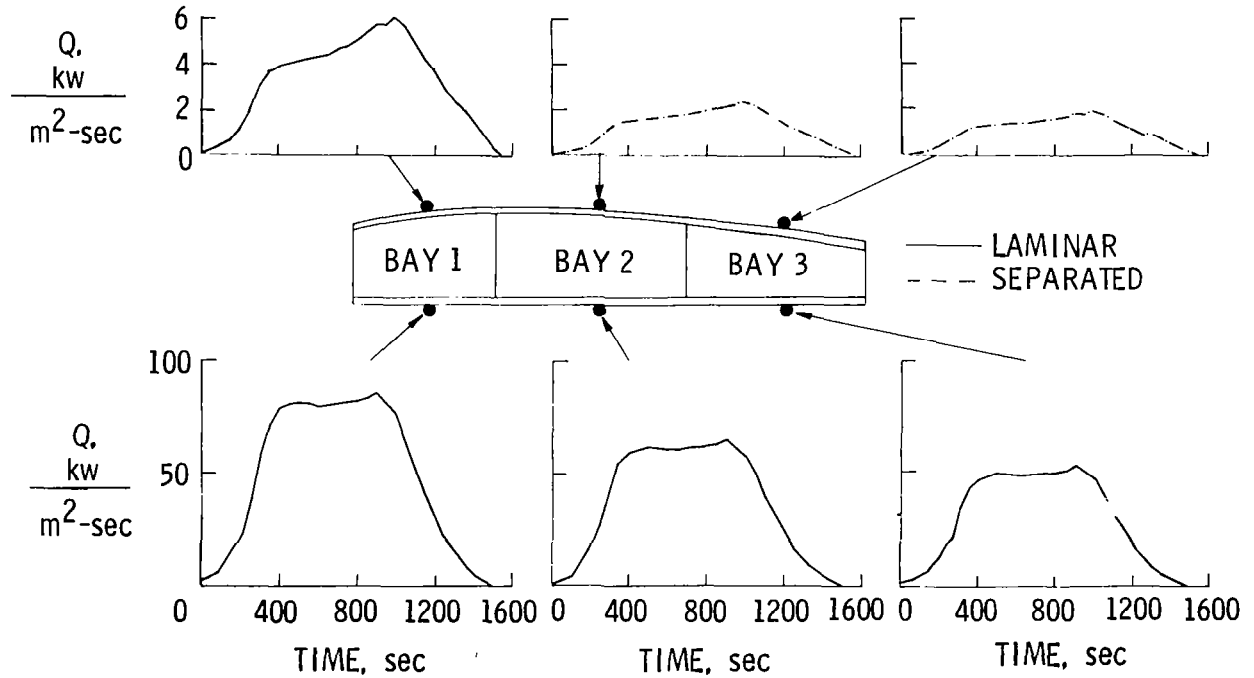


Figure 13.- Calculated heating rates, WS 328.

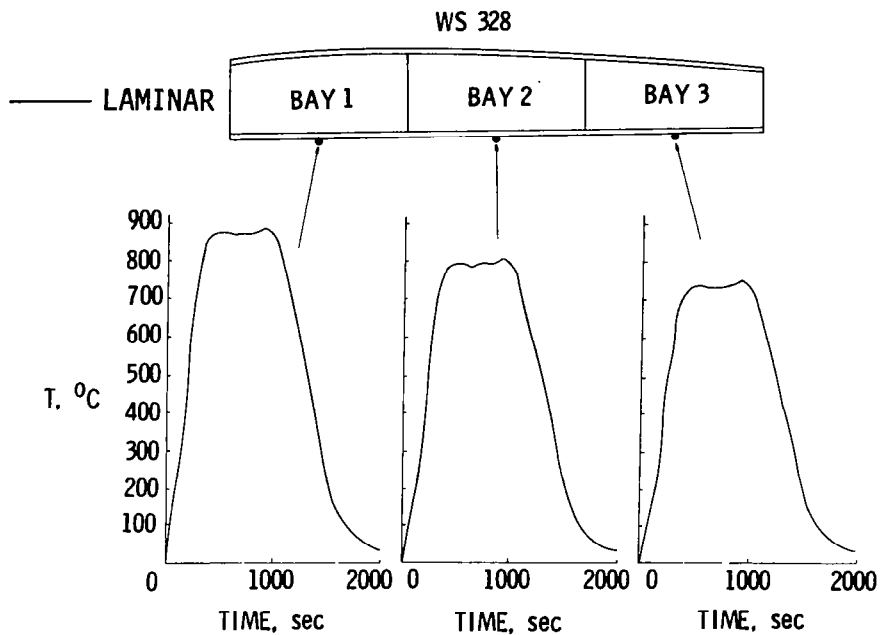


Figure 14.- Calculated surface temperatures of lower surface, WS 328.

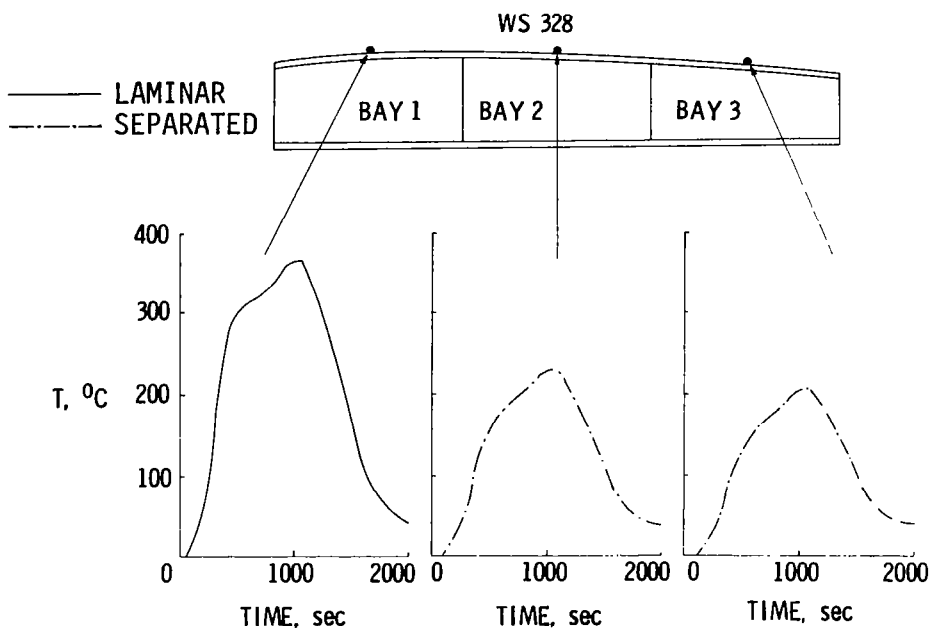


Figure 15.- Calculated surface temperatures of upper surface, WS 328

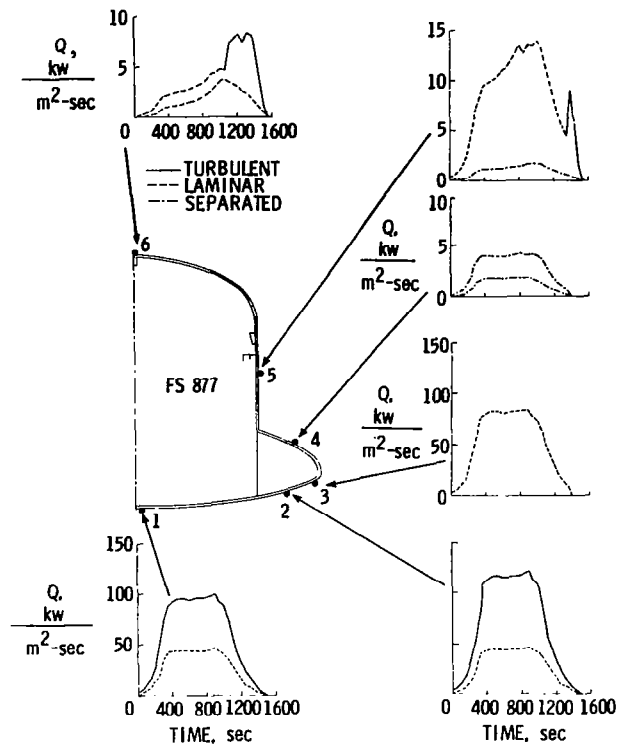


Figure 16.- Calculated heating rates, FS 877.

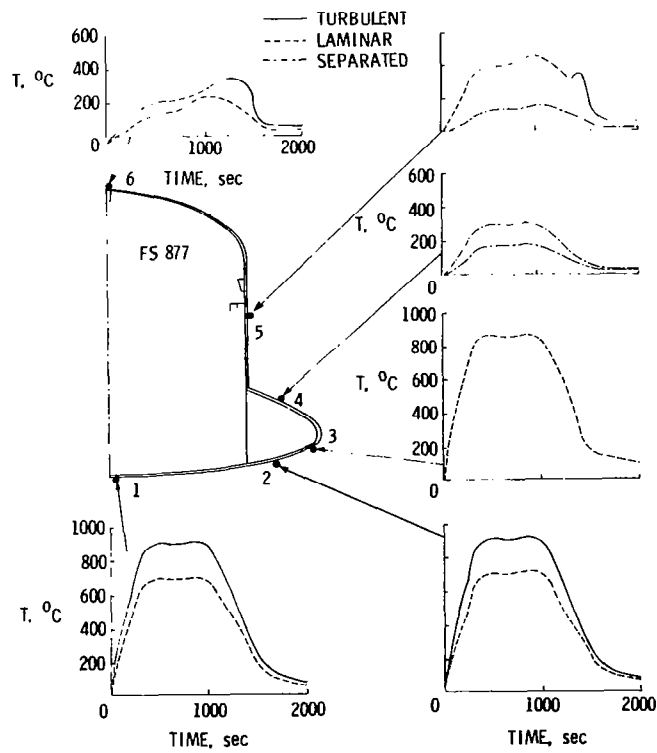


Figure 17.- Calculated surface temperatures at FS 877.

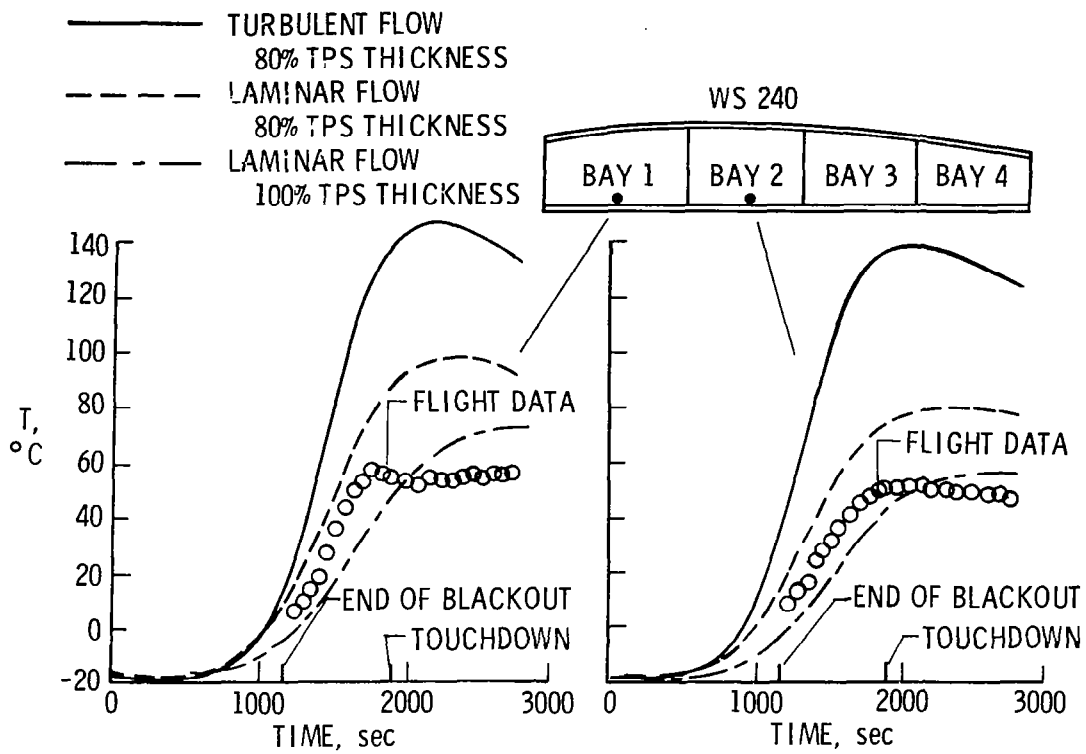


Figure 18.- Lower skin temperatures of bays 1 and 2, WS 240.

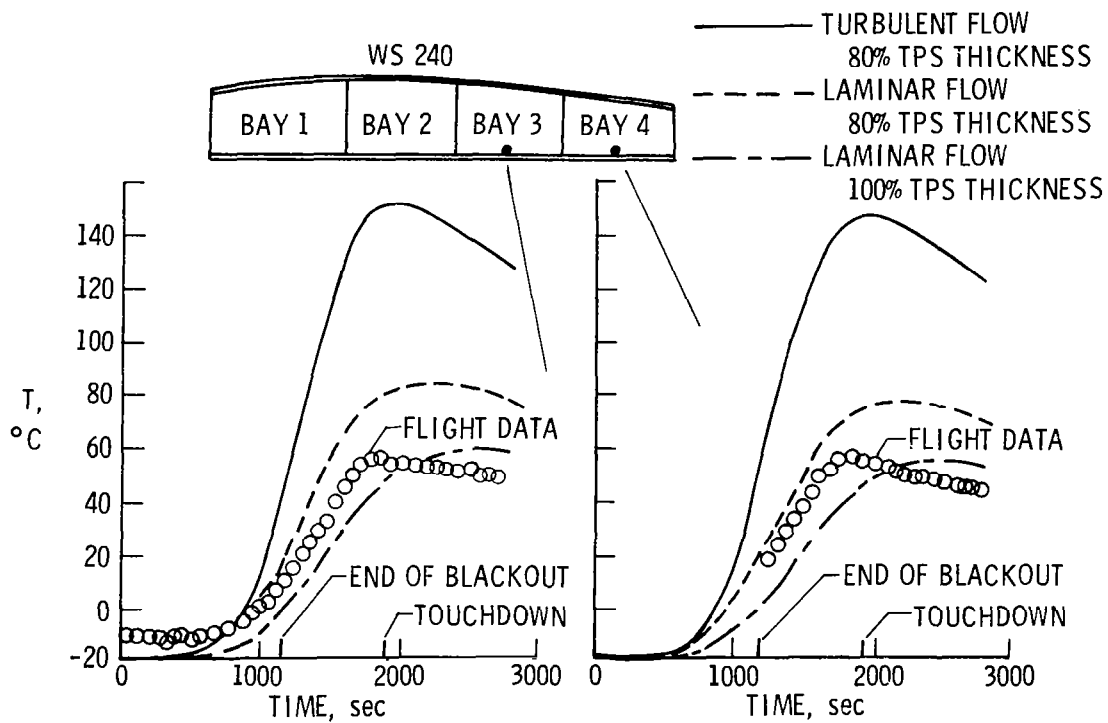


Figure 19.- Lower skin temperatures of bays 3 and 4, WS 240.

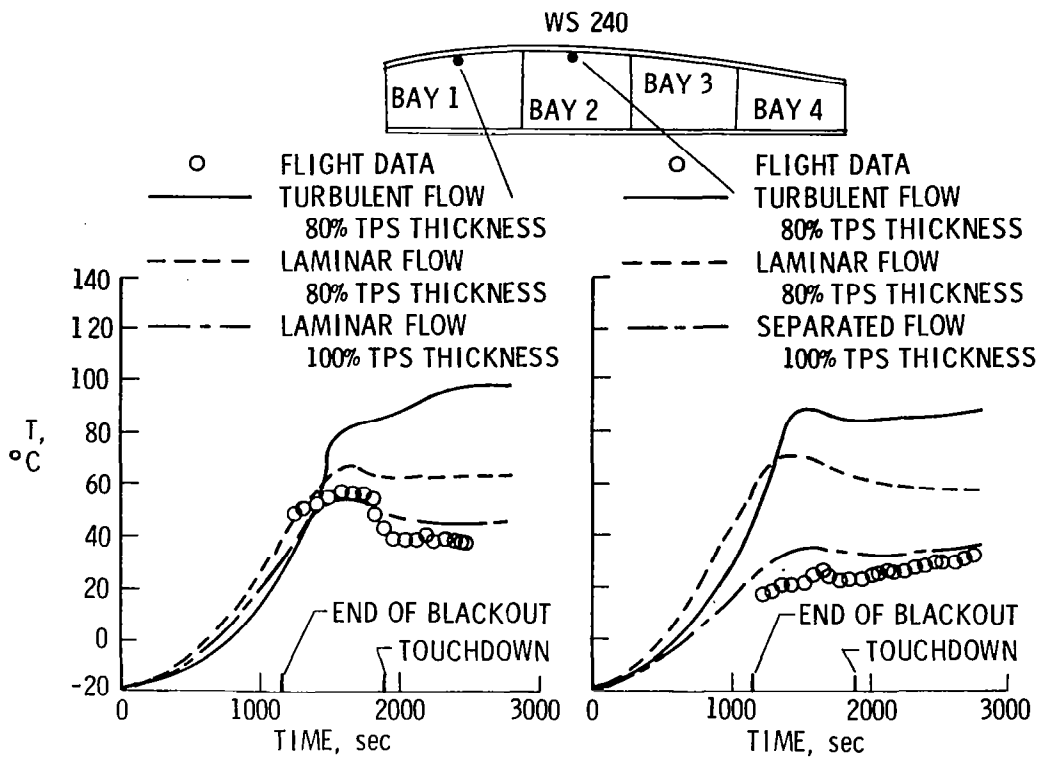


Figure 20.- Upper skin temperatures of bays 1 and 2, WS 240.

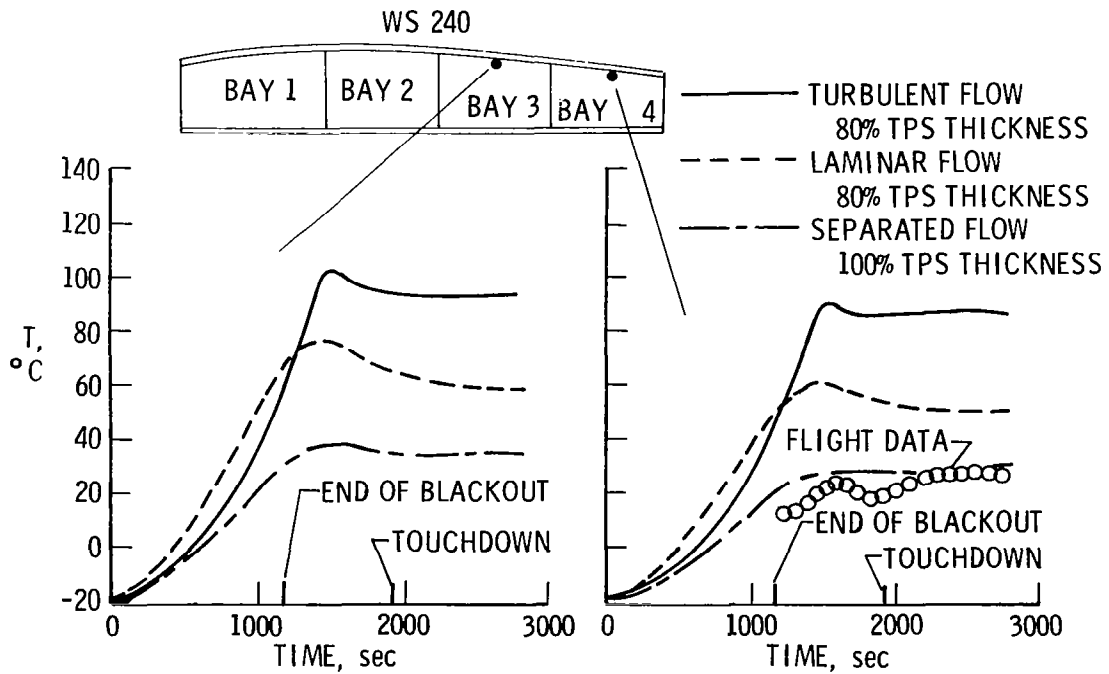


Figure 21.- Upper skin temperatures of bays 3 and 4, WS 240.

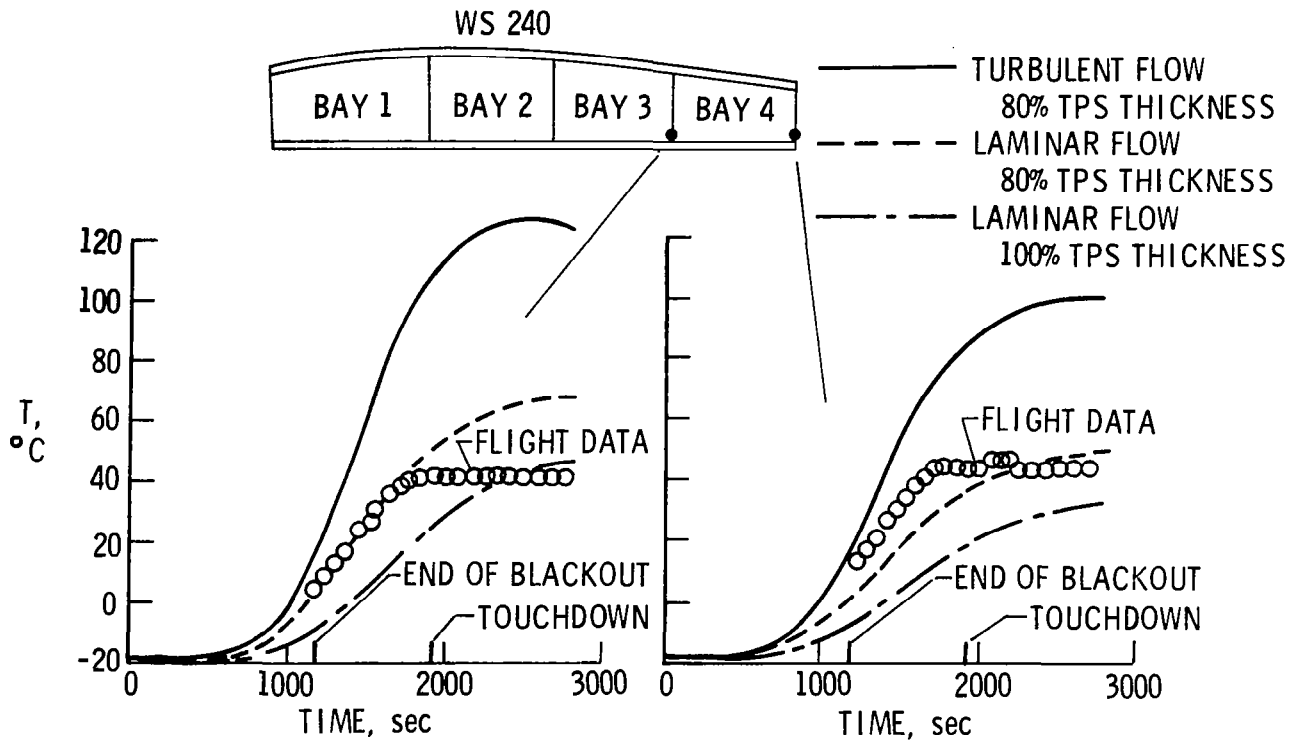


Figure 22.- Lower spar cap temperatures.

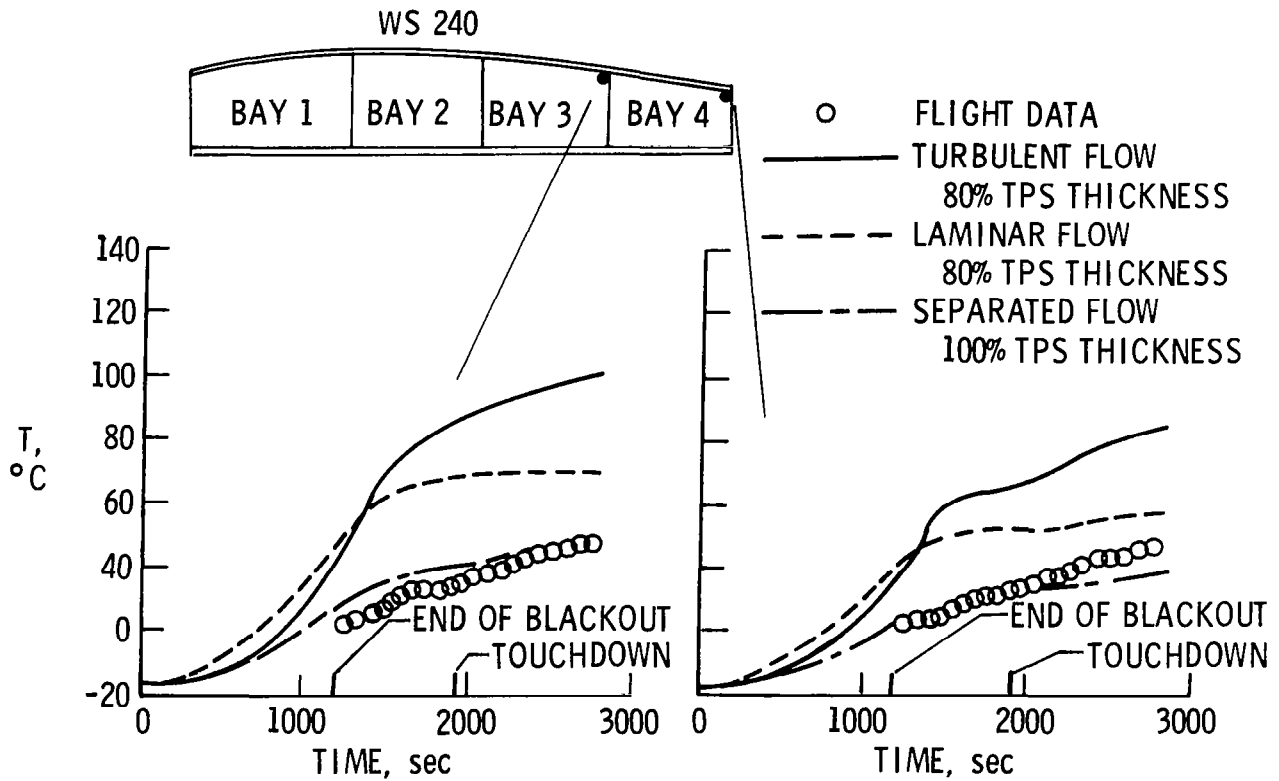


Figure 23.- Upper spar cap temperatures.